NeuroImage 278 (2023) 120277

Contents lists available at ScienceDirect

NeuroImage

journal homepage: www.elsevier.com/locate/ynimg

Functional alterations in bipartite network of white and grey matters during aging

Yurui Gao [a,b,*], Yu Zhao [a,c], Muwei Li [a,c], Richard D. Lawless [a,d], Kurt G. Schilling [a,c], Lyuan Xu [a,d], Andrea T. Shafer [e], Lori L. Beason-Held [e], Susan M. Resnick [e], Baxter P. Rogers [a,b,c,f], Zhaohua Ding [a,b,d,g], Adam W. Anderson [a,b], Bennett A. Landman [a,b,c,d,g], John C. Gore [a,b,c,*], for the Alzheimer's Disease Neuroimaging Initiative[1]

[a] Vanderbilt University Institute of Imaging Science, Vanderbilt University Medical Center, Nashville, TN, USA
[b] Department of Biomedical Engineering, Vanderbilt University, Nashville, TN, USA
[c] Department of Radiology and Radiological Sciences, Vanderbilt University Medical Center, Nashville, TN, USA
[d] Department of Electrical and Computer Engineering, Vanderbilt University, Nashville, TN, USA
[e] Laboratory of Behavioral Neuroscience, National Institute on Aging, National Institutes of Health, Baltimore, MD, USA
[f] Department of Psychiatry and Behavioral Sciences, Vanderbilt University Medical Center, Nashville, TN, USA
[g] Department of Computer Science, Vanderbilt University, Nashville, TN, USA

ARTICLE INFO

Keywords:
White matter
Resting state FMRI
Functional connectivity
Bipartite graph
Normal aging
Adulthood

ABSTRACT

The effects of normal aging on functional connectivity (FC) within various brain networks of gray matter (GM) have been well-documented. However, the age effects on the networks of FC between white matter (WM) and GM, namely WM-GM FC, remains unclear. Evaluating crucial properties, such as global efficiency (GE), for a WM-GM FC network poses a challenge due to the absence of closed triangle paths which are essential for assessing network properties in traditional graph models. In this study, we propose a bipartite graph model to characterize the WM-GM FC network and quantify these challenging network properties. Leveraging this model, we assessed the WM-GM FC network properties at multiple scales across 1,462 cognitively normal subjects aged 22–96 years from three repositories (ADNI, BLSA and OASIS-3) and investigated the age effects on these properties throughout adulthood and during late adulthood (age $\geq$70 years). Our findings reveal that (1) heterogeneous alterations occurred in region-specific WM-GM FC over the adulthood and decline predominated during late adulthood; (2) the FC density of WM bundles engaged in memory, executive function and processing speed declined with age over adulthood, particularly in later years; and (3) the GE of attention, default, somatomotor, frontoparietal and limbic networks reduced with age over adulthood, and GE of visual network declined during late adulthood. These findings provide unpresented insights into multi-scale alterations in networks of WM-GM functional synchronizations during normal aging. Furthermore, our bipartite graph model offers an extendable framework for quantifying WM-engaged networks, which may contribute to a wide range of neuroscience research.

1. Introduction

Normal aging has been associated with disrupted resting-state functional connectivity (rsFC) within various brain networks (Jockwitz and Caspers, 2021). The default mode network (DMN) is the most extensively investigated network in age-related studies. Researchers consistently observe lower rsFC measures with older age within the DMN, as well as attention networks (Andrews-Hanna et al., 2007; Betzel et al., 2014; Damoiseaux et al., 2008; Geerligs et al., 2015; Koch et al., 2010; Tomasi and Volkow, 2012; Zonneveld et al., 2019). In contrast,

* Corresponding authors at: Vanderbilt University Institute of Imaging Science, Vanderbilt University Medical Center, Nashville, TN, USA.
E-mail addresses: yurui.gao@vanderbilt.edu (Y. Gao), john.gore@vumc.org (J.C. Gore).

[1] Data used in preparation of this article were obtained from the Alzheimer's Disease Neuroimaging Initiative (ADNI) database (adni.loni.usc.edu). As such, the investigators within the ADNI contributed to the design and implementation of ADNI and/or provided data but did not participate in analysis or writing of this report. A complete listing of ADNI investigators can be found at: http://adni.loni.usc.edu/wp-content/uploads/how_to_apply/ADNI_Acknowledgement_List.pdf.

https://doi.org/10.1016/j.neuroimage.2023.120277
Received 14 April 2023; Received in revised form 23 June 2023; Accepted 11 July 2023
Available online 18 July 2023

opposite changes related to age have been reported in the frontoparietal network (FPN) (Betzel et al., 2014; Chan et al., 2014; Jockwitz and Caspers, 2021; Mowinckel et al., 2012), somatomotor network (SMN) (Stumme et al., 2020; Tomasi and Volkow, 2012), and visual network (VN) (Stumme et al., 2020; Varangis et al., 2019; Zonneveld et al., 2019). The age-related functional alterations in the limbic network (LN) (Achard and Bullmore, 2007) are less conclusive (See Table S1 for a mini literature summary). Notably, these age-related studies have limited their analyses to gray matter (GM) regions, without considering the other crucial functional complement in brain networks – white matter (WM).

Functional MRI (fMRI) signals of WM have been ignored for decades, partly because they are weaker due to the lower blood volume and flow in WM compared to GM (Helenius et al., 2003; Rostrup et al., 2000). Recently, a growing corpus of evidence indicates that blood oxygenation-level dependent (BOLD) fluctuations in fMRI signals from WM are reliably measurable using WM-tailored methods (see (Gore et al., 2019) for a review). For example, we recently showed that BOLD activations in WM can be measured voxel-wise by detecting increases in synchronization of fMRI signals along WM fibers instead of assuming a specific hemodynamic response to neural activity as is typical in GM activation mapping (Zhao et al., 2022b, 2022a). Extending beyond the voxel level, we have demonstrated that temporal correlations of resting state fMRI signals between WM and GM regions (i.e., WM-GM rsFC) are functionally relevant (Ding et al., 2018). Studies on clinical populations have confirmed that region-specific WM-GM rsFC is sensitive to a set of brain disorders, particularly age-related diseases such as Alzheimer's disease (AD) (Gao et al., 2020). However, whether and how the WM-GM rsFC metrics and networks change during normal aging remains unclear.

Investigating changes in the WM-GM rsFC networks poses a challenge due to the inadequacy of the conventional graph framework commonly used for analyzing GM-GM connection networks. This framework is not suited to efficiently characterize the WM-GM rsFC network and evaluate its important network properties. Specifically, unlike the GM-GM connection network where all nodes are GM nodes, the WM-GM rsFC network encompasses two distinct groups of nodes (i.e., WM and GM nodes) connected solely by inter-group links (i.e., WM-GM rsFC). The absence of within-group links (i.e., WM-WM and GM-GM rsFC) in the WM-GM FC network leads to the absence of closed triangular paths among any three nodes in the network (Borgatti and Everett, 1997), making it challenging to evaluate important network properties such as global efficiency (GE). Introducing WM-WM and/or GM-GM rsFC links into the WM-GM network may seem as a potential solution to generate triangular paths, but the validity of this approach is questionable due to differences in the underlying neurobiological mechanisms and amplitudes of the three types of rsFC, especially given the observations that BOLD fluctuation in WM is weaker and delayed than in GM (Gore et al., 2019). Moreover, mixed types of rsFC links make the derived network properties more difficult to interpret.

To address this methodological challenge, we propose a bipartite graph model that characterizes the unique topology of a WM-GM rsFC network and introduce a projection-based solution that evaluates its challenging network properties. Taking advantage of this novel method, we aim to investigate the age effects on WM-GM network properties during normal aging. Specifically, we assessed rsFC between atlas-defined WM bundles and GM parcels in a large cohort of cognitively healthy adults (N=1462, age=22–96 years) combined from three databases. We then measured FC density (FCD) of the WM bundles and GE of six predefined functional networks (i.e., DMN, FPN, LN, AN, SMN and VN) using our proposed graph model. Finally, we quantified age associations with these multi-scale measures during both entire adulthood and late adulthood. Our proposed model provides a framework for evaluating the network properties of the WM-GM rsFC graph, with potential contributions to a wide range of neuroscience research. Our analyses represent the first exploration of the multi-scale alterations in WM-GM rsFC networks during normal aging, enhancing our understanding of how WM-engaged brain networks age.

2. Methods

2.1. Data

Data in our study were aggregated from three databases: Alzheimer's Disease Neuroimaging Initiative – stages 2 and 3 (ADNI-2&3, https://adni.loni.usc.edu), Baltimore Longitudinal Study of Aging (BLSA, https://www.blsa.nih.gov) and Open Access Series of Imaging Studies – stage 3 (OASIS-3, https://www.oasis-brains.org). From each database, all baseline resting state fMRI (rsfMRI) images of cognitively normal subjects and their corresponding T1-weighted (T1w) images were downloaded in deidentified form, as well as demographic information, with IRB approval. A total of 1462 subjects (836 female, aged 22 to 96 years with mean of 69.1 ± 12.5 years) remained for final analyses (after preprocessing, quality control and harmonization described below). Please refer to supplementary method S1 for detailed descriptions of the three databases and supplementary Table S2 for imaging parameters and age distributions across all acquisition sites.

2.2. Preprocessing and quality control

An automatic high-performance pipeline was established to preprocess the large-scale data, as described extensively in our previous study (Gao et al., 2023; Li et al., 2023). Briefly, the rsfMRI images were corrected for slice timing and head motion effects. Consequently, 24 motion-related parameters (Friston et al., 1996) and the mean cerebrospinal fluid (CSF) signal were regressed out. The data were detrended and temporally filtered with a passband frequency of 0.01 - 0.1 Hz. All these steps were implemented using house-modified modules within the Data Processing Assistant for Resting-State fMRI toolbox (Yan et al., 2016). Tissue probability maps (TPM) for GM, WM and CSF were derived by segmenting the T1w images using the Computational Anatomy Toolbox (CAT12, https://neuro-jena.github.io/cat) (Gaser et al., 2022). Then, the rsfMRI data and TPMs were spatially normalized into MNI space using co-registration and normalization functions in SPM12 (https://www.fil.ion.ucl.ac.uk/spm/software/spm12) and CAT12. To suppress partial volume influences between WM and GM, no spatial smoothing was performed in the preprocessing. Of note, a test-retest experiment performed on OASIS-3 data (N=1000) confirmed the reliability of our pipeline, as evidenced by the intraclass correlation coefficients between rsFC of the test and retest groups (refer to (Gao et al., 2023) for more details).

The preprocessed results underwent a manual quality control procedure. The following passing criteria were applied: 1) successful generation of all the preprocessed results; 2) maximal translations and rotations of head motion less than 2 mm and 2°, respectively; 3) mean frame-wise displacement (FD) less than 0.5 mm (Power et al., 2012; Yan et al., 2013); and 4) expert visual inspection confirming acceptable spatial normalization.

2.3. Functional connectivity and harmonization

To generate the WM-GM rsFC matrix for each subject, Pearson's correlation coefficients were computed between regional time courses of fMRI signals from predefined WM bundles and GM parcels in MNI space. The WM bundles were defined by the JHU's ICBM-DTI-81 WM atlas (Mori et al., 2008) merged with refined cerebellar bundles delineated by van Baarsen et al. (van Baarsen et al., 2016). Due to poor signal quality and dropout, two small WM bundles (i.e., bilateral tapetums) were excluded from further analyses. The GM parcels were derived from the PickAtlas (Lancaster et al., 2000) which labeled Broadman areas. The atlas-defined WM and GM regions were further constrained within the whole-brain WM and GM masks of individual subjects, respectively. These masks were generated by thresholding the WM and GM TPMs at

0.8 to prevent signal contamination between WM and adjacent GM.

To reduce potential biases and non-biological influences of acquisition site effects, a ComBat (Johnson et al., 2007) harmonization procedure was performed on the rsFC values using the neuroComBat R package (https://github.com/Jfortin1/neuro Combat_Rpackage). Age and sex were included as covariates. Briefly, the ComBat model describes the rsFC values in the form $y_{ijv} = \alpha_v + X_{ij}\beta_v + \gamma_{iv} + \delta_{iv}\varepsilon_{ijv}$ where y_{ijv} is the rsFC of acquisition site i, subject j, and WM-GM pair v. The term α_v is the average rsFC of pair v, and X_{ij} is a design matrix for the covariates of interest. The terms γ_{iv} and δ_{iv} represent the additive and multiplicative site effects, respectively. ε_{ijv} is the residual term. The harmonized rsFC values were then computed as $y_{ijv}^{ComBat} = \frac{y_{ijv} - \widehat{\alpha}_v - X_{ij}\widehat{\beta}_v - \gamma_{iv}^*}{\delta_{iv}^*} + \widehat{\alpha}_v + X_{ij}\widehat{\beta}_v$, where γ_{iv}^* and δ_{iv}^* are the empirical Bayes estimates. Of note, the inclusion of age and sex as covariates in the harmonization process ensured retention of the rsFC variations associated with age and sex. Any single subject within one site was removed before this procedure. Previous studies have demonstrated that ComBat adjustment outperforms methods that merely include site as a nuisance covariate (Fortin et al., 2018; Yu et al., 2018).

2.4. Bipartite graph and WM-GM rsFC connectome measures

A bipartite graph, also known as a two-mode graph or bigraph, $\mathcal{G} = (W, G, E, B)$ comprises two distinct groups of nodes, W ($|W| = m$) and G ($|G| = n$), with a set of links, E, connecting nodes between the two groups (Newman et al., 2001). In our specific context, the WM bundles and GM parcels were designated as the two groups of nodes, represented by $w_i \in W$ and $g_j \in G$, respectively. The WM-GM rsFC were designated as the undirected weighted link, e_{ij}, connecting nodes w_i and g_j. Of note, there are no links between any within-group nodes. This bipartite graph can be efficiently represented by a weighted biadjacency matrix, B, where the element at the ith row (corresponding to w_i) and the jth column (corresponding to g_j), b_{ij}, represents the weight of link e_{ij}, as illustrated by a simple model in Fig. 1A. Based on this weighted bipartite graph, the following attributes were computed to measure connectome properties of WM-GM rsFC. Refer to supplementary method S2 for more details.

2.4.1. FC density of WM bundle

FC density (FCD) of a WM bundle, w_i, is defined as the averaged rsFC between the WM bundle and all GM nodes. This measurement quantified the rsFC strength of each WM bundle connections to the entire cerebral cortex. From the perspective of classic graph analysis, the FCD of w_i can be considered a node strength (Barrat et al., 2004) normalized by the number of GM nodes, formalized as follows:

$$FCD(w_i) = \frac{1}{n}\sum_{j}^{n} b_{ij}. \tag{1}$$

2.4.2. Global efficiency of functional network

Global efficiency (GE) is an important system-level property, that measures the overall efficiency of information integration in a brain functional network. However, it cannot be directly derived from the WM-GM rsFC graph due to the absence of triangular paths. To address this issue, we projected the original bipartite network to a directed weighted unipartite network where only GM nodes were explicitly present and WM nodes were hidden. In this projected network, two GM nodes (g_j and g_j) were considered connected only if they shared at least one common WM node, w_p, in the original bipartite network. The adjacency matrix of the projected network, denoted as $A = (a_{jj})_{n\times n}$ (Fig. 1A), was obtained by transforming from the biadjacency matrix B into A using the following definition:

$$a_{jj} = \begin{cases} \sum_p b_{pj} \ (b_{pj} \neq 0,\ b_{pj} \neq 0,\ j \neq j) \\ 0 \ (j = j) \end{cases}. \tag{2}$$

Based on this transformation, the connectivity from a starting GM node, g_j, to an ending GM node, g_j, in the projected network was determined by summing the original rsFC between the starting GM node and all the WM nodes shared by the two GM nodes. Therefore, we refer to this projected network as the "WM-mediated GM-GM network". To provide a simplified example of the bipartite-to-unipartite projection for easier understanding, consider Fig. 1B, where GM nodes g_3 and g_4 share two common WM nodes w_3 and w_4 in the bipartite graph. Consequently, the WM-mediated link from g_3 towards g_4 is weighted by the sum of b_{33} and b_{43}, denoted as a_{34} in the projected graph. Likewise, the weight of the link from g_4 towards g_3 is the sum of b_{34} and b_{44}, denoted as a_{43}.

All GM nodes were categorized into six functional networks according to Yeo's functional parcellation of cerebral cortex (Yeo et al., 2011), including DMN, FPN, LN, AN (combination of dorsal and ventral ANs), SMN and VN, as shown in Fig. 1C. Specifically, each GM parcel was assigned to one of the networks depending on which network had the largest overlap with the parcel. The GE of the kth functional network N_k, was then calculated based on the following equation:

$$GE(N_k) = \frac{1}{n_k(n_k-1)}\sum_{j}^{n_k}\sum_{j,j\neq j}^{n_k}\left(d_{jj}\right)^{-1} \ (n_k = num\ of\ nodes\ in\ N_k), \tag{3}$$

where d_{jj} is the shortest weighted path between g_j and g_j described

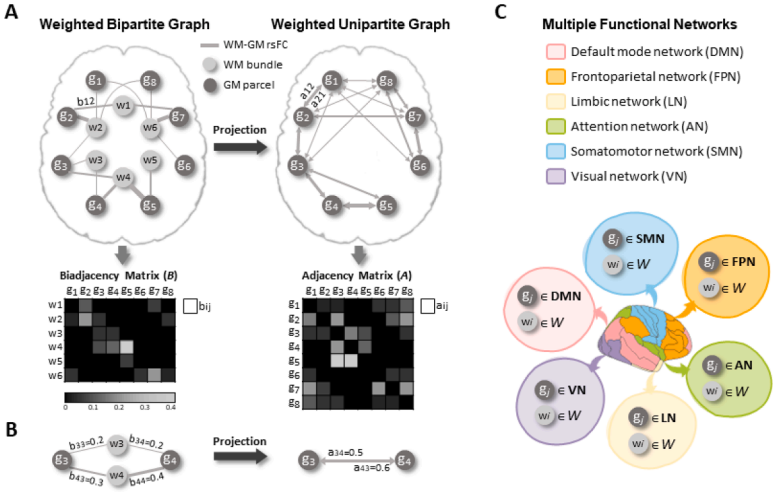

Fig. 1. | A conceptual model illustrating bipartite graph, graph projection, and design of network analysis. (A) Projection from a WM-GM rsFC weighted bipartite graph to a WM-mediated weighted unipartite graph and the corresponding transformation of biadjacency matrix towards adjacency matrix. (**B**) An example to show the algorithm in projection. (**C**) Design of functional network analysis based on graph projection. Note that although only GM nodes are present in the projected graph, the inter-node connections in the graph are still determined by the WM-GM rsFC.

elsewhere (Latora and Marchiori, 2001; Rubinov and Sporns, 2010). The GE value is typically the inverse of the average shortest path length in the network. In our context, it quantifies the level of integration of the WM-mediated GM-GM network.

Prior to the network analysis, each individual bipartite graph was threshold at 0.1 to remove spurious WM-GM rsFC. The lower value of 0.1 was chosen as a threshold because WM-GM rsFC tends to be lower than conventional GM-GM rsFC. In the validation analysis, we assessed the potential influence of the rsFC threshold on age effects on network properties by considering two adjacent thresholds 0.05 and 0.15.

2.5. Statistical analysis

To investigate age effects on WM functional measures, we modeled the trajectory of rsFC for each WM-GM pair or FCD for each WM bundle over the entire adulthood using multiple linear regression. We considered both linear and quadratic models with sex and head motion (i.e., mean Power's FD, Power et al., 2012) as covariates:

$$y = \beta_0^{lin} + \beta_1^{lin} \times age + \beta_2^{lin} \times sex + \beta_3^{lin} \times FD + \epsilon \quad (4)$$

and

$$y = \beta_0^{qua} + \beta_1^{qua} \times age + \beta_2^{qua} \times age^2 + \beta_3^{qua} \times sex + \beta_4^{qua} \times FD + \epsilon, \quad (5)$$

where y is rsFC or FCD. T-tests on parameter β_1^{lin} or β_2^{qua} were conducted to ascertain whether the models exhibited statistically significant age effects. The resulting p-value were adjusted for multiple comparisons using the false discovery rate (FDR) (Benjamini and Hochberg, 1995), yielding q-values. The model that best described the adulthood trajectory was selected based on Akaike information criterion (Akaike, 1974). We reported standardized β_1^{lin} or β_2^{qua} of the best-fit model for each rsFC or FCD of bundle in the results section. For rsFC or FCD exhibiting a significant quadratic age effect, the peak age was further determined as follows:

$$age_{peak} = \frac{-\beta_1^{qua}}{2\beta_2^{qua}} \quad (6)$$

Moreover, we further modeled the age effects in late adulthood (age $\geq$ 70 years) because the age effect might be more manifest in older adults.

The age effects on the GE of each WM-mediated functional network were modeled with multiple linear regression, as depicted in Eq. (4), and the p-values were corrected for 6 comparisons using Bonferroni correction.

3. Results

3.1. Demography and harmonization

A total of 1462 subjects (836 female, 57%) were included in the final analyses after quality control and harmonization. The age range of the subjects spanned from early and middle adulthood, with a denser distribution in late adulthood (Fig. 2A). Specifically, the numbers of subjects across decades are 15 for 22–29 years, 27 for 30–39 years, 74 for 40–49 years, 171 for 50–59 years, 399 for 60–69 years, 498 for 70–79 years, 253 for 80–90 years and 25 for 90–96 years.

Possible site-effects on WM-GM rsFC were effectively corrected by the harmonization process which mitigated mean and variance differences across 53 sites, as illustrated in the comparison of rsFC before and after harmonization for a randomly selected WM-GM pair (Fig. 2B). The group-level WM-GM rsFC matrices for the three databases after harmonization (Fig. 2C) exhibited highly similar patterns, indicating the stability of WM-GM functional connectivity architectures at rest and the reliability of our pipeline for measuring rsFC within a large cohort from multiple databases. Moreover, compared to the ADNI-2&3 and BLSA (age=76±7 and 67±15 years, respectively) groups, the rsFC in the OASIS-3 group mean matrix (age=68±9 years) appears sharper, as evidenced by slightly hotter red and cooler blue colors, Fig. 2C), suggesting preserved age-related variances after harmonization.

3.2. Age effects on rsFC of WM-GM pairs

Our model fitting results revealed three major significant age effects ($q < 0.05$) on rsFC between atlas-defined WM bundles and GM parcels (Fig. 3D) over adulthood: a negative linear age effect ($\beta_1^{lin} < 0$), a positive linear age effect ($\beta_1^{lin} > 0$) and an inverted-U-shaped age effect ($\beta_2^{qua} < 0$) (Fig. 3A). The proportions of WM-GM pairs with the three effects among all pairs with significant age effects were 20.6%, 41.5% and 37.6%, respectively (Fig. 3C). The peak ages of the inverted-U-shaped age effects ranged from 46 to 80 years (mean of 63±6 years, Fig. S1). By contrast, rsFC during late adulthood exhibited predominantly negative linear age effects (99.2%) with only a small number of positive linear effects (0.8%, Fig. 3BC). Comparing the distributions of age effects between adulthood and late adulthood suggests a more pronounced

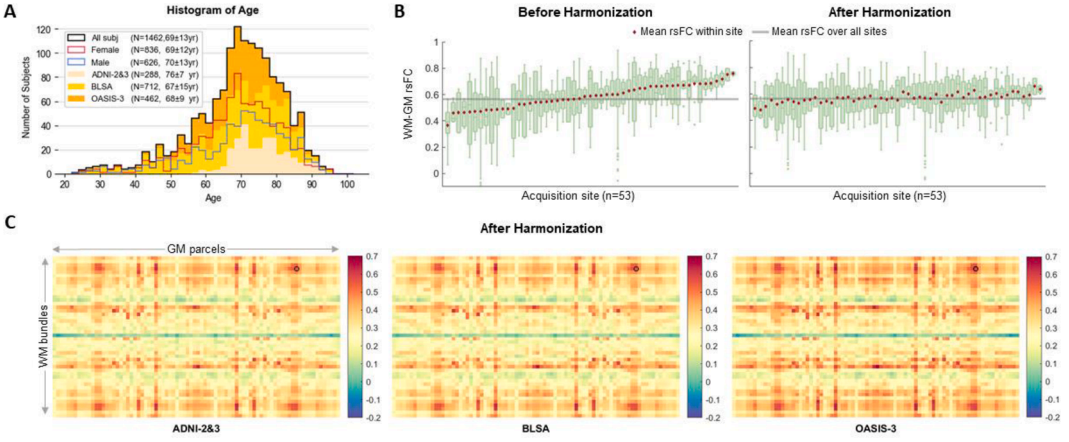

Fig. 2. | Histogram of age, comparison before and after harmonization, and mean WM-GM rsFC matrices of three databases after harmonization. (A) Age distributions of all subjects analyzed in our study. The distributions of the three databases are stacked. (**B**) Comparison of summary statistics (including median, 0.25 and 0.75 quartiles, nonoutlier minimum and maximum, and outliers) of a randomly selected WM-GM rsFC for 53 acquisition sites before and after harmonization. The red diamond indicates the mean rsFC within a site. The semi-transparent gray line serves as a reference for the mean rsFC over all sites. (**C**) Group mean matrices of WM-GM rsFC for the three databases after site-effect removal, exhibiting highly repeated patterns. The black circles indicate the location of the selected rsFC exanimated in (B).

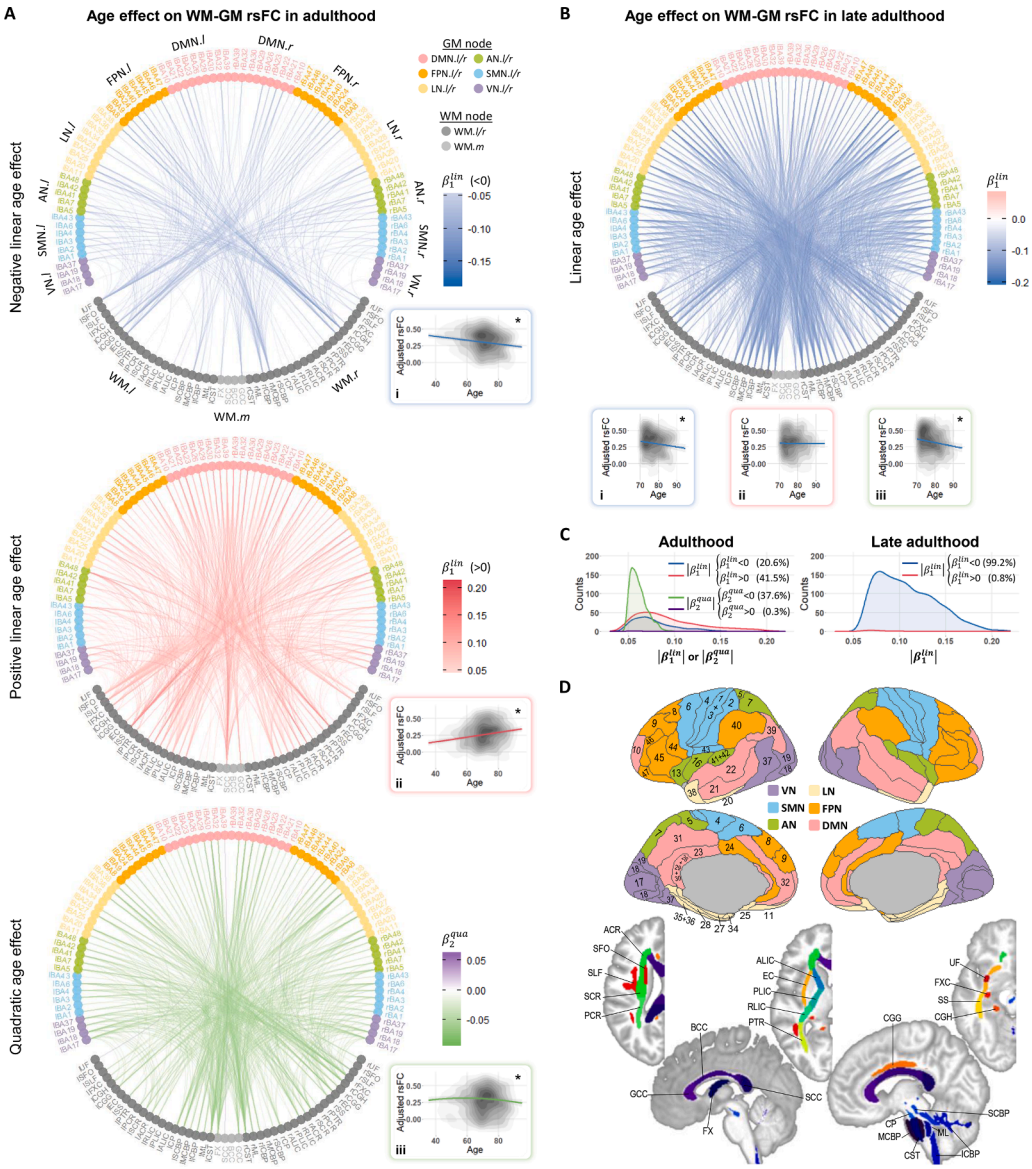

Fig. 3. | Age effects on rsFC of WM-GM pairs. (A) Significant age effects on WM-GM rsFC over entire adulthood ($q < 0.05$). Each colored node represents a GM parcel assigned to a functional network and each gray node represents a WM bundle. Blue and red curves in the first and second circles indicate negative and positive linear trends of rsFC between WM bundles and GM parcels over age, respectively. The green and purple curves in the third circle indicate inverted-U- and U-shaped quadratic relationships between rsFC and age, respectively. (**B**) Linear age effects on rsFC during late adulthood ($q < 0.01$ for clearer visualization). Boxes **(i), (ii)** and **(iii)** in (A, B) illustrate three representative WM-GM pairs, showing linear and quadratic trajectories during entire adulthood (boxes in A) and late adulthood (boxes in B) overlaid on kernel density plots of data points. (**C**) Distributions of β_1^{lin} and β_2^{qua} for entire adulthood fitting and β_1^{lin} for late adulthood fitting. (D) GM parcels (Brodmann areas) color-coded based on their affiliated functional networks (i.e., DMN, FPN, LN, AN, SMN or VN) and deep WM bundles defined by atlases. See Table S3 for more WM descriptions.

decline in rsFC during late adulthood (Fig. 3C). This observation is further supported by the rsFC of three representative WM-GM pairs (boxes i, ii and iii in Fig. 1A and 1B): the rsFC between the right cingulum beneath the cingulate gyrus (CGG) and right Brodmann area (BA) 38, between the splenium of corpus callosum (SCC) and BA47, and between the left bilateral corticospinal tract (CST) and right BA4. They exhibited negative linear ($\beta_1^{lin} = -0.19$, $q < 0.01$), positive linear ($\beta_1^{lin} = 0.20$, $q < 0.01$) and inverted-U-shaped quadratic age effects ($\beta_2^{qua} = -0.05$, $q < 0.05$, peak age = 64 years) over the entire adult lifespan, respectively, but showed negative ($\beta_1^{lin} = -0.14$, $q < 0.01$), insignificant ($\beta_1^{lin} = -0.005$, $q = 0.29$) and negative linear ($\beta_1^{lin} = -0.14$, $q < 0.01$) age effects during late adulthood, respectively.

3.3. Age effects on FCD of WM bundles

Across the entire adult lifespan, three significant age effects were observed on FCD of WM bundles (inner circle in Fig. 4A and Table S3). Specifically, eight WM bundles exhibited negative linear age-related variations in FCD ($q < 0.05$), including the fornix (FX) ($\beta_1^{lin} = -0.12$, $q < 0.01$, Fig. 4B), bilateral CGG ($\beta_1^{lin} = -0.08$, $q < 0.01$ and $\beta_1^{lin} = -0.11$, $q < 0.01$ for the left and right bundles, respectively), right middle cerebellar peduncles (MCBP) ($\beta_1^{lin} = -0.08$, $q = 0.01$), right external capsules (EC) ($\beta_1^{lin} = -0.08$, $q < 0.01$), left uncinate fasciculus (UF) ($\beta_1^{lin} = -0.08$, $q = 0.01$), right inferior cerebellar peduncles (ICBP) ($\beta_1^{lin} = -0.07$, $q = 0.02$) and right fornix cres (FXC) ($\beta_1^{lin} = -0.07$, $q = 0.02$). Another nine WM bundles also exhibited linear age effects but with positive polarity, including the SCC ($\beta_1^{lin} = 0.17$, $q < 0.01$, Fig. 4B), bilateral sagittal stratum (SS) ($\beta_1^{lin} = 0.13$, $q < 0.01$ and $\beta_1^{lin} = 0.08$, $q < 0.01$), left posterior thalamic radiation (PTR) ($\beta_1^{lin} = 0.12$, $q < 0.01$), bilateral anterior corona radiata (ACR) ($\beta_1^{lin} = 0.08$, $q < 0.01$ and $\beta_1^{lin} = 0.09$, $q < 0.01$), left superior longitudinal fasciculus (SLF) ($\beta_1^{lin} = 0.07$, $q = 0.01$), left retrolenticular part of internal capsule RLIC ($\beta_1^{lin} = 0.07$, $q = 0.02$) and left superior fronto-occipital fasciculus (SFO) ($\beta_1^{lin} = 0.06$, $q = 0.046$). Meanwhile, four WM bundles showed significant quadratic age effects (inverted-U-shaped trajectories), including bilateral CST ($\beta_2^{qua} = -0.07$, $q < 0.01$ for both, Fig. 4B), left superior cerebellar peduncle (SCBP) ($\beta_2^{qua} = -0.06$, $q < 0.01$) and left medial lemniscus (ML) ($\beta_2^{qua} = -0.05$, $q = 0.04$).

During late adulthood, all WM bundles exhibited negative linear age effects to some extent (outer circle in Fig. 4A and Table S3). Twenty-four bundles exhibited significant linear declines with age ($q < 0.05$),

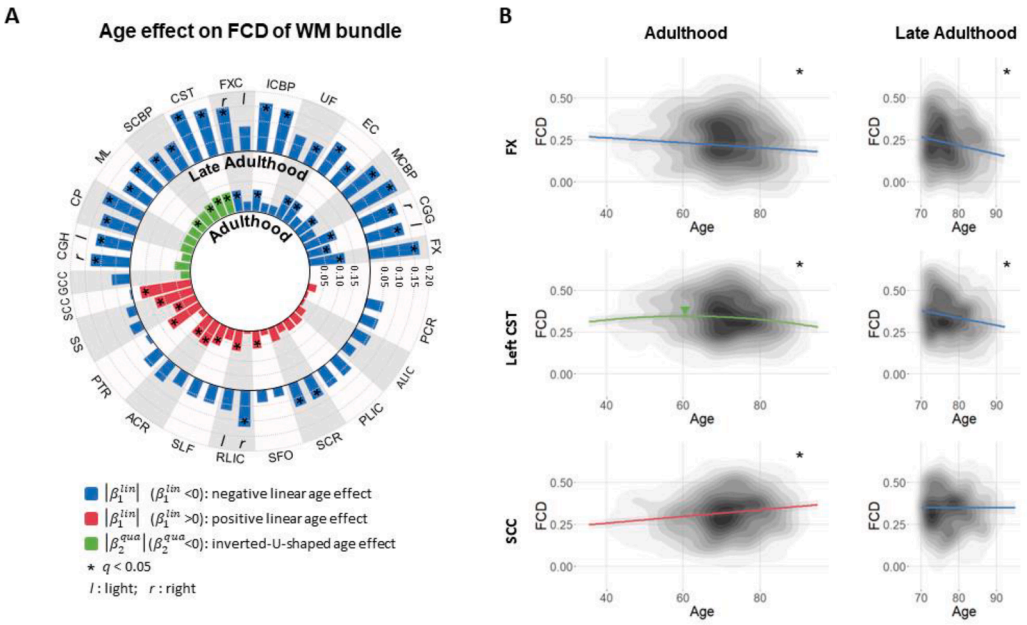

Fig. 4. | Age effects on rsFC density (FCD) of WM bundles. (A) Age effect on FCD of each WM bundle over entire adulthood (bars at inner circle) and late adulthood (bars at outer circle). Blue and red bars indicate negative and positive linear age effects, respectively. Green bars indicate inverted-U-shaped age effects. The height of each bar represents β_1^{lin} or β_2^{qua}. An asterisk on the bar indicates $q < 0.05$. (**B**) Three examples showing trajectories of FCD over adulthood (left column) and late adulthood (right column). The β_1^{lin} or β_2^{qua} and corresponding q values for all WM bundles are summarized in Table S3.

including the FX (Fig. 4B), bilateral CGG, MCBP, EC, ICBP, CST (Fig. 4B), SCBP, ML, cerebral peduncle (CP), cingulum at hippocampus (CGH), superior corona radiata (SCR), left UF, right FXC and RLIC.

3.4. Age effects on GE of functional networks

To investigate how normal aging affects the overall communication efficiency within WM-GM functional networks, we evaluated the GE of six pre-defined functional networks (i.e., DMN, FPN, LN, AN, SMN and VN) by projecting WM-GM rsFC bipartite graphs to WM-mediated GM-GM rsFC unipartite graphs. The resulting GE values of five networks were found associated with age to different extents over the entire adulthood (Fig. 5A-E). Specifically, we found significant negative relations with age for these networks, among which the DMN ($\beta = -0.10$, $p < 0.01$), FPN ($\beta = -0.09, p < 0.01$), AN ($\beta = -0.11, p < 0.01$), SMN ($\beta = -0.12, p < 0.01$) exhibited stronger age-related decline and the LN ($\beta = -0.08$, $p = 0.014$) showed a slightly weaker decline. Although no significant age-related association with GE across the entire adulthood was found for the VN ($\beta = -0.03, p = 0.22$), the age effect on GE of VN in late adulthood was significant ($\beta = -0.10$, $p = 0.02$) (Fig. 5F, G). Moreover, validation analyses using lower and higher thresholds for graph construction yielded similar results (Fig. S3). Collectively, these results converged to suggest that aging broadly affected the functional integrations of multiple WM-mediated networks in the brain.

4. Discussion

In this large-scale multi-cohort study, we aimed to identify age effects on WM-GM functional interactions in brain during normal aging from both local and systemic perspectives. We hypothesized that the architecture of WM-GM rsFC networks would alter with age, supported by observations of age-related structural degradations in WM (Cox et al., 2016; O'Sullivan et al., 2001) and disturbed WM-GM rsFC in changes with cognition during the development of Alzheimer's disease (Gao et al., 2019). However, assessing crucial network properties of a WM-GM rsFC graph, such as GE, has been difficult due to the absence of closed triplets in such a graph. Our work primarily demonstrates (i) a proposed novel method including construction of a graph specifically tailored to the unique nature of WM-GM rsFC and assessment of the network properties; (ii) evidence of age-related alterations in WM-GM rsFC and FCD of WM-bundles over long-range adulthood or in late adulthood (age $\geq$ 70 years); and (iii) evidence of loss of integration in six WM-mediated functional networks during aging, occurring with varying extent and onset. The implications of these findings are expanded below,

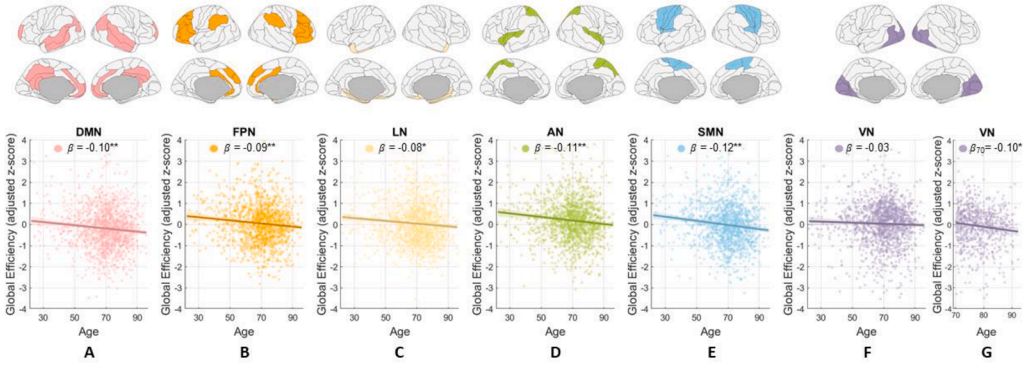

Fig. 5. | Age associations with global efficiency (GE, adjusted z-score) of six WM-mediated functional networks. The upper plots highlight the GM parcels assigned to each functional network, namely default mode network (DMN), fronto-parietal network (FPN), limbic network (LN), attention network (AN), somatomotor network (SMN), and visual network (VN). In the lower plots, the regression line with 95% confidence intervals shown for each network indicates the relationship of GE with age throughout the entire adulthood. The value β represents standardized coefficient of age in multiple linear regression over the entire adulthood, and β_{70} over late adulthood. * indicates $p < 0.05$ and ** indicates $p < 0.01$, corrected for multiple comparisons.

as well as the limitations of the methods.

4.1. Extendable bipartite WM-GM rsFC model

To our knowledge, this study represents the first attempt to introduce a bipartite graph model for characterizing the WM-GM rsFC network and evaluating the challenging network property, GE, through bipartite-to-unipartite projection. In the projected WM-mediated GM-GM network, other challenging properties such as clustering coefficient can also be readily evaluated. Moreover, the projection is not limited to the transformation defined by Eq. (2). Alternative transformations can be easily applied in a similar manner.

Previous studies investigating WM-GM FC for brain abnormalities, including neuropsychiatric disorder and neurodegenerative disease (Gao et al., 2021, 2020; Liu et al., 2022; Yang et al., 2020), have focused on exploring less challenging network properties. In contrast, our bipartite model enables researchers to assess broader network properties, thereby expected to have wide prospects for applications.

4.2. Patterns of age-related alterations

Throughout the core measurements in our study (i.e., rsFC of WM-GM pairs, FCD of WM bundles and GE of projection of WM-GM networks), we found at least three common patterns of age-related functional alterations – reductions in adulthood, reductions in late-adulthood and relative stability of function with age. These contrasting patterns hint that aging influences certain WM functional architectures disproportionately. Similar patterns have also been mentioned explicitly or implicitly in previous reports on GM-GM rsFC changes (Andrews-Hanna et al., 2007; Jockwitz and Caspers, 2021) and age-related behavioral alterations (Hedden and Gabrieli, 2004).

4.3. Degradations of WM bundles

The WM bundles exhibiting significantly lower FCD towards aging in this study, regardless of the adulthood period in which they occur, have been associated with cognition, sensory-motor processing, and visual perception. Specifically, half of the bundles (i.e., FX, FXC, CGG, CGH, UF, EC and SCR) are frontal-parietal-temporal or frontal-temporal fibers and have been demonstrated to play important roles in higher-order cognitions such as episodic/working memory, executive control and emotion, all of which decline with age (Bendlin et al., 2010; Bubb et al., 2018; Douet and Chang, 2015; Hedden and Gabrieli, 2004; McLaughlin et al., 2003; O'Sullivan et al., 2001; Papagno et al., 2011). The remaining bundles (i.e., MCBP, ICBP, CST, SCBP, ML, CP and RLIC) have been mainly associated with sensory-motor processing and visual processing (Johns, 2014; Kim et al., 2014; Morales and Tomsick, 2015; Navarro-Orozco and Bollu, 2022; Ribas et al., 2018), both of which also show declines in aging regarding processing speed of motor responses and visuospatial ability to complete complex tasks (Navarro-Orozco and Bollu, 2022; Salthouse, 2010). Therefore, our observations contribute further evidence of the neural substrates underlying age-related cognitive declines.

These observed WM-bundle-wise changes in BOLD synchronization may be driven by several factors. First, age-related microstructural changes detected by diffusion MRI (Barrick et al., 2010; Bendlin et al., 2010; Burzynska et al., 2010; Cox et al., 2016; Davis et al., 2009), probably reflecting loss of axons and demyelination (Salvadores et al., 2017), have been reported in WM, and may impact the WM function. Second, deterioration and volume loss in the GM parcels connected to the WM bundles during aging could also play a role (Marstaller et al., 2015). Third, BOLD fluctuations depend on cerebral blood flow and metabolism (Tsvetanov et al., 2015), and PET/MRI evidence has shown reduced baseline cerebral blood flow in elder populations (Martin et al., 1991; Stoquart-ElSankari et al., 2007). Moreover, these factors may be intertwined. For example, the disturbance in the rsFC between CGG and BA32 (dorsal anterior cingulate cortex) might be partially caused by age-related effects such as disrupted CGG microstructure, decreased cingulate volume, reduced metabolism and cerebral blood flow (Mann et al., 2011; Pardo et al., 2007; Vaidya et al., 2007; Westlye et al., 2010).

Interestingly, the FCD of bundles SCC, SS, PTR, ACR, SLF, RLIC and SFO were found to be positively affected by age across adulthood, despite the microstructural impairments reported in these bundles with age (Barrick et al., 2010; Bendlin et al., 2010; Cox et al., 2016). Several of these bundles also overlap with common regions of age-related WM hyperintensities (Habes et al., 2018), which may affect FC measures (Jaywant et al., 2022; Tsvetanov et al., 2015). This observation suggests the presence of an over-recruitment or/and compensation mechanism via network reorganization in WM, similar to the over-recruitments of GM regions reported at rest and during cognitive tasks (Grady et al., 2016). In addition, significant increases in these bundles were absent during late adulthood and may be due to increased degeneration of underlying tissues such as neurons, axons, synapses or/and vasculature that occurs with more advanced age.

4.4. Dissolved integration of WM-mediated networks

In one WM-mediated network, a reduced GE implies disrupted or even absent communication between nodes within the network. Our results indicate that as the brain ages, all six networks lose their ability to efficiently combine information from distributed parts, especially the DMN, AN and SMN, which agrees with previous aging studies using conventional GM-GM graphs at rest (refer to Table S1 for a mini summary of the relevant literature and two reviews (Deery et al., 2023; Jockwitz and Caspers, 2021). At least some of the age-dependent declines in GE may be driven by alterations in anatomical connectivity and energy demands (Salat, 2011).

Taking the rsFC-wise, bundle-wise and network-wise observations together, we may speculate on how the WM architecture reflects overall brain function. For example, we found FCD of the bundles SCC and SS increased with age as did the rsFC between these bundles and GM nodes in DMN. The functional integration of the WM-mediated DMN, as well as all other networks, still decreased however, suggesting that local compensation may not always suffice to prevent global deterioration of a functional circuit.

4.5. Limitations

In the present study, (Newman et al., 2001) the WM bundles utilized were relatively thick units and were delineated based on diffusion tractography-inferred anatomy (Mori et al., 2008). Several WM bundles, such as the fornix and cingulum, anatomically branch into more than one cortical region along their individual fiber pathways (Schmahmann and Pandya, 2009), suggesting that a single WM bundle may functionally contribute to multiple networks. Therefore, we included all WM bundles in each functional network for graph construction and GE assessment. Further investigation into a more refined bundle delineation that allows for a finer 'functional resolution' could be worthwhile.

Additionally, it is important to note that fMRI measures in both GM and WM are inherently indirect measures of neural activity, depending on neurovascular coupling. Changes in vascular properties in the brain and hemodynamic responses to energy demands may occur independently of changes in neural activity. Therefore, caution should be exercised when interpreting the results.

5. Conclusions

In conclusion, this study presents an extendable graph model that characterizes the unique nature and measures challenging properties of the WM-GM rsFC network. Based on this model, the study also presents large-scale analyses, revealing that WM-GM rsFC and FCD of WM bundles associated to higher-order cognition and sensory-motor processing

undergo age-related declines during adulthood. The same metrics of w WM bundles predominantly decline in late adulthood. At the system level, the DMN, AN, SMN, FPN, LN and VN all exhibit reduced functional cohesiveness with age, with varying extents during adulthood or late adulthood. This study fills both methodological and knowledge gaps in the WM-GM FC network of the aging human brain, providing insights into the missing piece – WM-engaged function – in the puzzle of the human connectome.

Acknowledgments

The project is supported by National Institute of Mental Health grant (1RF1MH123201, Gore and Landman), National Institute of Neurological Disorders and Stroke grant (R01NS113832, Gore), Vanderbilt Discovery Grant (FF600670, Gao), grant of Vanderbilt Institute for Clinical and Translational Research (UL1TR0002243) and by Intramural Research Program of the National Institute on Aging of the NIH. We also thank the Vanderbilt Advanced Computing Center for Research and Education (ACCRE) and VUIIS-XNAT and DAX teams.

ADNI data collection and sharing for this project was funded by NIH grant U01 AG024904, DOD award W81XWH-12–2–0012. ADNI is funded by the National Institute on Aging, the National Institute of Biomedical Imaging and Bioengineering, and through generous contributions from the following: AbbVie, Alzheimer's Association; Alzheimer's Drug Discovery Foundation; Araclon Biotech; BioClinica, Inc.; Biogen; Bristol-Myers Squibb Company; CereSpir, Inc.; Cogstate; Eisai Inc.; Elan Pharmaceuticals, Inc.; Eli Lilly and Company; EuroImmun; F. Hoffmann-La Roche Ltd and its affiliated company Genentech, Inc.; Fujirebio; GE Healthcare; IXICO Ltd.; Janssen Alzheimer Immunotherapy Research & Development, LLC.; Johnson & Johnson Pharmaceutical Research & Development LLC.; Lumosity; Lundbeck; Merck & Co., Inc.; Meso Scale Diagnostics, LLC.; NeuroRx Research; Neurotrack Technologies; Novartis Pharmaceuticals Corporation; Pfizer Inc.; Piramal Imaging; Servier; Takeda Pharmaceutical Company; and Transition Therapeutics. The Canadian Institutes of Health Research is providing funds to support ADNI clinical sites in Canada. Private sector contributions are facilitated by the Foundation for the National Institutes of Health (www.fnih.org). The grantee organization is the Northern California Institute for Research and Education, and the study is coordinated by the Alzheimer's Therapeutic Research Institute at the University of Southern California. ADNI data are disseminated by the Laboratory for Neuro Imaging at the University of Southern California.

Data and code availability statements

The ADNI data can be downloaded through LONI at http://adni.loni.usc.edu/data-samples/access-data/ (application/review is needed).

The OASIS3 data can be downloaded through XNAT at https://central.xnat.org/data/projects/OASIS3 (application/review is needed).

The BLSA data can be downloaded through at https://www.blsa.nih.gov (application/review is needed)

The codes for establishment of fMRI / T1 preprocessing pipeline can be downloaded from https://github.com/VUIIS/SCZ-WM-pipeline?organization=VUIIS&organization=VUIIS

The Combat harmonization package can be downloaded from https://github.com/Jfortin1/neuroCombat_Rpackage

The codes (R/Python/Matlab) created by authors for visualizing results in this study will be uploaded to Github under first author's repository (https://github.com/gaoy3/bipartite) and open to public after acceptance of this manuscript.

CRediT authorship contribution statement

Yurui Gao: Conceptualization, Methodology, Formal analysis, Investigation, Data curation, Writing – original draft, Visualization. **Yu Zhao:** Methodology, Writing – review & editing. **Muwei Li:** Software. **Richard D. Lawless:** Software. **Kurt G. Schilling:** Data curation. **Lyuan Xu:** Methodology. **Andrea T. Shafer:** Data curation, Writing – review & editing. **Lori L. Beason-Held:** Data curation, Writing – review & editing. **Susan M. Resnick:** Data curation, Writing – review & editing. **Baxter P. Rogers:** Software, Methodology, Resources, Writing – review & editing. **Zhaohua Ding:** Conceptualization, Methodology. **Adam W. Anderson:** Conceptualization, Resources. **Bennett A. Landman:** Conceptualization, Resources, Data curation, Writing – review & editing, Supervision, Project administration, Funding acquisition. **John C. Gore:** Conceptualization, Writing – review & editing, Supervision, Project administration, Funding acquisition.

Declaration of Competing Interest

All authors declare no known competing financial interests or personal relationships with other people or organizations that could inappropriately influence the work reported in this paper.

Data availability

I have shared the link to my data/code at the attach file step.

Supplementary materials

Supplementary material associated with this article can be found, in the online version, at doi:10.1016/j.neuroimage.2023.120277.

References

Achard, S., Bullmore, E., 2007. Efficiency and cost of economical brain functional networks. PLoS Comput. Biol. 3 https://doi.org/10.1371/journal.pcbi.0030017 e17–e17.

Akaike, H., 1974. A new look at the statistical model identification. IEEE Trans. Automat. Contr. 19, 716–723. https://doi.org/10.1109/TAC.1974.1100705.

Andrews-Hanna, J.R., Snyder, A.Z., Vincent, J.L., Lustig, C., Head, D., Raichle, M.E., Buckner, R.L., 2007. Disruption of large-scale brain systems in advanced aging. Neuron 56, 924–935. https://doi.org/10.1016/j.neuron.2007.10.038.

Barrat, A., Barthélemy, M., Pastor-Satorras, R., Vespignani, A., 2004. The architecture of complex weighted networks. Proc. Natl. Acad. Sci. U. S. A. 101, 3747–3752. https://doi.org/10.1073/pnas.0400087101.

Barrick, T.R., Charlton, R.A., Clark, C.A., Markus, H.S., 2010. White matter structural decline in normal ageing: a prospective longitudinal study using tract-based spatial statistics. Neuroimage 51, 565–577. https://doi.org/10.1016/j.neuroimage.2010.02.033.

Bendlin, B.B., Fitzgerald, M.E., Ries, M.L., Xu, G., Kastman, E.K., Thiel, B.W., Rowley, H. A., Lazar, M., Alexander, A.L., Johnson, S.C., 2010. White matter in aging and cognition: a cross-sectional study of microstructure in adults aged eighteen to eighty-three. Dev. Neuropsychol. 35, 257–277. https://doi.org/10.1080/87565641003696775.

Benjamini, Y., Hochberg, Y., 1995. Controlling the false discovery rate: a practical and powerful approach to multiple testing. J. R. Stat. Soc. Series B Stat. Methodol. 57, 289–300. https://doi.org/10.1111/j.2517-6161.1995.tb02031.x.

Betzel, R.F., Byrge, L., He, Y., Goñi, J., Zuo, X.N., Sporns, O., 2014. Changes in structural and functional connectivity among resting-state networks across the human lifespan. Neuroimage 102, 345–357. https://doi.org/10.1016/j.neuroimage.2014.07.067.

Borgatti, S.P., Everett, M.G., 1997. Network analysis of 2-mode data. Soc. Netw. 19, 243–269. https://doi.org/10.1016/S0378-8733(96)00301-2.

Bubb, E.J., Metzler-Baddeley, C., Aggleton, J.P., 2018. The cingulum bundle: anatomy, function, and dysfunction. Neurosci. Biobehav. Rev. 92, 104–127. https://doi.org/10.1016/j.neubiorev.2018.05.008.

Burzynska, A.Z., Preuschhof, C., Bäckman, L., Nyberg, L., Li, S.C., Lindenberger, U., Heekeren, H.R., 2010. Age-related differences in white matter microstructure: region-specific patterns of diffusivity. Neuroimage 49, 2104–2112. https://doi.org/10.1016/j.neuroimage.2009.09.041.

Chan, M.Y., Park, D.C., Savalia, N.K., Petersen, S.E., Wig, G.S., 2014. Decreased segregation of brain systems across the healthy adult lifespan. Proc. Natl. Acad. Sci. 111, E4997–E5006. https://doi.org/10.1073/pnas.1415122111.

Cox, S.R., Ritchie, S.J., Tucker-Drob, E.M., Liewald, D.C., Hagenaars, S.P., Davies, G., Wardlaw, J.M., Gale, C.R., Bastin, M.E., Deary, I.J., 2016. Ageing and brain white matter structure in 3,513 UK Biobank participants. Nat. Commun. 7, 13629. https://doi.org/10.1038/ncomms13629.

Damoiseaux, J.S., Beckmann, C.F., Arigita, E.J.S., Barkhof, F., Scheltens, Ph., Stam, C.J., Smith, S.M., Rombouts, S.A.R.B., 2008. Reduced resting-state brain activity in the "default network" in normal aging. Cereb. Cortex 18, 1856–1864. https://doi.org/10.1093/cercor/bhm207.

Davis, S.W., Dennis, N.A., Buchler, N.G., White, L.E., Madden, D.J., Cabeza, R., 2009. Assessing the effects of age on long white matter tracts using diffusion tensor tractography. Neuroimage 46, 530–541. https://doi.org/10.1016/j.neuroimage.2009.01.068.

Deery, H.A., Di Paolo, R., Moran, C., Egan, G.F., Jamadar, S.D., 2023. The older adult brain is less modular, more integrated, and less efficient at rest: a systematic review of large-scale resting-state functional brain networks in aging. Psychophysiology 60, e14159. https://doi.org/10.1111/psyp.14159.

Ding, Z., Huang, Y., Bailey, S.K., Gao, Y., Cutting, L.E., Rogers, B.P., Newton, A.T., Gore, J.C., 2018. Detection of synchronous brain activity in white matter tracts at rest and under functional loading. Proc. Natl. Acad. Sci. U. S. A. 115 https://doi.org/10.1073/pnas.1711567115.

Douet, V., Chang, L., 2015. Fornix as an imaging marker for episodic memory deficits in healthy aging and in various neurological disorders. Front. Aging Neurosci. 6 https://doi.org/10.3389/fnagi.2014.00343.

Fortin, J.P., Cullen, N., Sheline, Y.I., Taylor, W.D., Aselcioglu, I., Cook, P.A., Adams, P., Cooper, C., Fava, M., McGrath, P.J., McInnis, M., Phillips, M.L., Trivedi, M.H., Weissman, M.M., Shinohara, R.T., 2018. Harmonization of cortical thickness measurements across scanners and sites. Neuroimage 167, 104–120. https://doi.org/10.1016/j.neuroimage.2017.11.024.

Friston, K.J., Williams, S., Howard, R., Frackowiak, R.S.J., Turner, R., 1996. Movement-related effects in fMRI time-series. Magn. Reson. Med. 35 https://doi.org/10.1002/mrm.1910350312.

Gao, Y., Lawless, D., Li, M., Zhao, Y., Schilling, K., Xu, L., Shafer, A., Beason-Held, L., Resnick, S., Rogers, B., Ding, Z., Anderson, A., Landman, B., Gore, J., 2023. Automatic preprocessing pipeline for white matter functional analyses of large-scale databases. In: Proc. SPIE, p. 124640U. https://doi.org/10.1117/12.2653132.

Gao, Y., Li, M., Huang, A.S., Anderson, A.W., Ding, Z., Heckers, S.H., Woodward, N.D., Gore, J.C., 2021. Lower functional connectivity of white matter during rest and working memory tasks is associated with cognitive impairments in schizophrenia. Schizophr. Res. 233, 101–110. https://doi.org/10.1016/j.schres.2021.06.013.

Gao, Y., Li, M., Zu, Z., Rogers, B.P., Anderson, A.W., Ding, Z., Gore, J.C., 2019. Progressive degeneration of white matter functional connectivity in Alzheimer's disease. In: Proc. SPIE, p. 109530C. https://doi.org/10.1117/12.2512919.

Gao, Y., Sengupta, A., Li, M., Zu, Z., Rogers, B.P., Anderson, A.W., Ding, Z., Gore, J.C., 2020. Functional connectivity of white matter as a biomarker of cognitive decline in Alzheimer's disease. PLoS One 15, e0240513. https://doi.org/10.1371/journal.pone.0240513.

Gaser, C., Dahnke, R., Thompson, P., Kurth, F., Luders, E., Alzheimer's Disease Neuroimaging Initiative, 2022. CAT – A computational anatomy toolbox for the analysis of structural MRI data. bioRxiv. https://doi.org/10.1101/2022.06.11.495736.

Geerligs, L., Renken, R.J., Saliasi, E., Maurits, N.M., Lorist, M.M., 2015. A brain-wide study of age-related changes in functional connectivity. Cereb. Cortex 25, 1987–1999. https://doi.org/10.1093/cercor/bhu012.

Gore, J.C., Li, M., Gao, Y., Wu, T.L., Schilling, K.G., Huang, Y., Mishra, A., Newton, A.T., Rogers, B.P., Chen, L.M., Anderson, A.W., Ding, Z., 2019. Functional MRI and resting state connectivity in white matter - a mini-review. Magn. Reson. Imaging 63. https://doi.org/10.1016/j.mri.2019.07.017.

Grady, C., Sarraf, S., Saverino, C., Campbell, K., 2016. Age differences in the functional interactions among the default, frontoparietal control, and dorsal attention networks. Neurobiol. Aging 41, 159–172. https://doi.org/10.1016/j.neurobiolaging.2016.02.020.

Habes, M., Erus, G., Toledo, J.B., Bryan, N., Janowitz, D., Doshi, J., Völzke, H., Schminke, U., Hoffmann, W., Grabe, H.J., Wolk, D.A., Davatzikos, C., 2018. Regional tract-specific white matter hyperintensities are associated with patterns of aging-related brain atrophy via vascular risk factors, but also independently. Alzheimer's Dement. Diagn. Assess. Dis. Monit. 10, 278–284. https://doi.org/10.1016/j.dadm.2018.02.002.

Hedden, T., Gabrieli, J.D.E., 2004. Insights into the ageing mind: a view from cognitive neuroscience. Nat. Rev. Neurosci. 5, 87–96. https://doi.org/10.1038/nrn1323.

Helenius, J., Perkiö, J., Soinne, L., Østeroaard, L., Carano, R.A.D., Salonen, O., Savolainen, S., Kaste, M., Aronen, H.J., Tatlisumak, T., 2003. Cerebral hemodynamics in a healthy population measured by dynamic susceptibility contrast MR imaging. Acta Radiol. 44 https://doi.org/10.1034/j.1600-0455.2003.00104.x.

Jaywant, A., Dunlop, K., Victoria, L.W., Oberlin, L., Lynch, C.J., Respino, M., Kuceyeski, A., Scult, M., Hoptman, M.J., Liston, C., O'Dell, M.W., Alexopoulos, G.S., Perlis, R.H., Gunning, F.M., 2022. Estimated regional white matter hyperintensity burden, resting state functional connectivity, and cognitive functions in older adults. Am. J. Geriatr. Psychiatry 30, 269–280. https://doi.org/10.1016/j.jagp.2021.07.015.

Jockwitz, C., Caspers, S., 2021. Resting-state networks in the course of aging—Differential insights from studies across the lifespan vs. amongst the old. Pflugers Arch. 473, 793–803. https://doi.org/10.1007/s00424-021-02520-7.

Johns, P., Johns, P., 2014. Chapter 3 - Functional neuroanatomy. Clinical Neuroscience 27–47. https://doi.org/10.1016/B978-0-443-10321-6.00003-5.

Johnson, W.E., Li, C., Rabinovic, A., 2007. Adjusting batch effects in microarray expression data using empirical Bayes methods. Biostatistics 8, 118–127. https://doi.org/10.1093/biostatistics/kxj037.

Kim, M.S., Tak, H.J., Son, S.M., 2014. Recovery of cerebellar peduncle injury in a patient with a cerebellar tumor: validation by diffusion tensor tractography. Neural. Regen. Res. 9, 1929–1932. https://doi.org/10.4103/1673-5374.145364.

Koch, W., Teipel, S., Mueller, S., Buerger, K., Bokde, A.L.W., Hampel, H., Coates, U., Reiser, M., Meindl, T., 2010. Effects of aging on default mode network activity in resting state fMRI: does the method of analysis matter? Neuroimage 51, 280–287. https://doi.org/10.1016/j.neuroimage.2009.12.008.

Lancaster, J.L., Woldorff, M.G., Parsons, L.M., Liotti, M., Freitas, C.S., Rainey, L., Kochunov, P.V., Nickerson, D., Mikiten, S.A., Fox, P.T., 2000. Automated Talairach Atlas labels for functional brain mapping. Hum. Brain Mapp. 10 https://doi.org/10.1002/1097-0193(200007)10:3<120::AID−HBM30>3.0.CO;2-8.

Latora, V., Marchiori, M., 2001. Efficient behavior of small-world networks. Phys. Rev. Lett. 87, 198701 https://doi.org/10.1103/PhysRevLett.87.198701.

Li, M., Gao, Y., Lawless, R.D., Xu, L., Zhao, Y., Schilling, K.G., Ding, Z., Anderson, A.W., Landman, B.A., Gore, J.C., 2023. Changes in white matter functional networks across late adulthood. Front. Aging Neurosci. 15 https://doi.org/10.3389/fnagi.2023.1204301.

Liu, N., Lencer, R., Yang, Z., Zhang, W., Yang, C., Zeng, J., Sweeney, J.A., Gong, Q., Lui, S., 2022. Altered functional synchrony between gray and white matter as a novel indicator of brain system dysconnectivity in schizophrenia. Psychol. Med. 52, 2540–2548. https://doi.org/10.1017/S0033291720004420.

Mann, S.L., Hazlett, E.A., Byne, W., Hof, P.R., Buchsbaum, M.S., Cohen, B.H., Goldstein, K.E., Haznedar, M.M., Mitsis, E.M., Siever, L.J., Chu, K.W., 2011. Anterior and posterior cingulate cortex volume in healthy adults: effects of aging and gender differences. Brain Res. 1401, 18–29. https://doi.org/10.1016/j.brainres.2011.05.050.

Marstaller, L., Williams, M., Rich, A., Savage, G., Burianová, H., 2015. Aging and large-scale functional networks: white matter integrity, gray matter volume, and functional connectivity in the resting state. Neuroscience 290, 369–378. https://doi.org/10.1016/j.neuroscience.2015.01.049.

Martin, A.J., Friston, K.J., Colebatch, J.G., Frackowiak, R.S.J., 1991. Decreases in regional cerebral blood flow with normal aging. J. Cereb. Blood Flow Metab. 11, 684–689. https://doi.org/10.1038/jcbfm.1991.121.

McLaughlin, C.T., Kane, A.G., Auber, A.E., 2003. MR imaging of heat stroke: external capsule and thalamic T1 shortening and cerebellar injury. Am. J. Neuroradiol. 24, 1372.

Morales, H., Tomsick, T., 2015. Middle cerebellar peduncles: magnetic resonance imaging and pathophysiologic correlate. World J. Radiol. 7, 438–447. https://doi.org/10.4329/wjr.v7.i12.438.

Mori, S., Oishi, K., Jiang, H., Jiang, L., Li, X., Akhter, K., Hua, K., Faria, A.V., Mahmood, A., Woods, R., Toga, A.W., Pike, G.B., Neto, P.R., Evans, A., Zhang, J., Huang, H., Miller, M.I., van Zijl, P., Mazziotta, J., 2008. Stereotaxic white matter atlas based on diffusion tensor imaging in an ICBM template. Neuroimage 40, 570–582. https://doi.org/10.1016/j.neuroimage.2007.12.035.

Mowinckel, A.M., Espeseth, T., Westlye, L.T., 2012. Network-specific effects of age and in-scanner subject motion: a resting-state fMRI study of 238 healthy adults. Neuroimage 63, 1364–1373. https://doi.org/10.1016/j.neuroimage.2012.08.004.

Navarro-Orozco, D., Bollu, P.C., 2022. Neuroanatomy, medial lemniscus (Reils Band, Reils Ribbon). StatPearls [Internet]. StatPearls, Treasure Island (FL).

Newman, M.E.J., Strogatz, S.H., Watts, D.J., 2001. Random graphs with arbitrary degree distributions and their applications. Phys. Rev. E 64, 26118. https://doi.org/10.1103/PhysRevE.64.026118.

O'Sullivan, M., Jones, D.K., Summers, P.E., Morris, R.G., Williams, S.C.R., Markus, H.S., 2001. Evidence for cortical "disconnection" as a mechanism of age-related cognitive decline. Neurology 57, 632. https://doi.org/10.1212/WNL.57.4.632.

Papagno, C., Miracapillo, C., Casarotti, A., Romero Lauro, L.J., Castellano, A., Falini, A., Casaceli, G., Fava, E., Bello, L., 2011. What is the role of the uncinate fasciculus? Surgical removal and proper name retrieval. Brain 134, 405–414. https://doi.org/10.1093/brain/awq283.

Pardo, J.V., Lee, J.T., Sheikh, S.A., Surerus-Johnson, C., Shah, H., Munch, K.R., Carlis, J. V., Lewis, S.M., Kuskowski, M.A., Dysken, M.W., 2007. Where the brain grows old: decline in anterior cingulate and medial prefrontal function with normal aging. Neuroimage 35, 1231–1237. https://doi.org/10.1016/j.neuroimage.2006.12.044.

Power, J.D., Barnes, K.A., Snyder, A.Z., Schlaggar, B.L., Petersen, S.E., 2012. Spurious but systematic correlations in functional connectivity MRI networks arise from subject motion. Neuroimage 59, 2142–2154. https://doi.org/10.1016/j.neuroimage.2011.10.018.

Ribas, E.C., Yağmurlu, K., de Oliveira, E., Ribas, G.C., Rhoton, A., 2018. Microsurgical anatomy of the central core of the brain. J. Neurosurg. 129, 752–769. https://doi.org/10.3171/2017.5.JNS162897.

Rostrup, E., Law, I., Blinkenberg, M., Larsson, H.B.W., Born, A.P., Holm, S., Paulson, O. B., 2000. Regional differences in the CBF and BOLD responses to hypercapnia: a combined PET and fMRI study. Neuroimage 11, 87–97. https://doi.org/10.1006/nimg.1999.0526.

Rubinov, M., Sporns, O., 2010. Complex network measures of brain connectivity: uses and interpretations. Neuroimage 52, 1059–1069. https://doi.org/10.1016/j.neuroimage.2009.10.003.

Salat, D.H., 2011. The declining infrastructure of the aging brain. Brain Connect 1, 279–293. https://doi.org/10.1089/brain.2011.0056.

Salthouse, T.A., 2010. Selective review of cognitive aging. J. Int. Neuropsychol. Soc. 16, 754–760. https://doi.org/10.1017/S1355617710000706.

Salvadores, N., Sanhueza, M., Manque, P., Court, F.A., 2017. Axonal degeneration during aging and its functional role in neurodegenerative disorders. Front. Neurosci. 11 https://doi.org/10.3389/fnins.2017.00451.

Schmahmann, J.D., Pandya, D.N., 2009. Fiber Pathways of the Brain. Oxford University Press, USA.

Stoquart-ElSankari, S., Balédent, O., Gondry-Jouet, C., Makki, M., Godefroy, O., Meyer, M.E., 2007. Aging effects on cerebral blood and cerebrospinal fluid flows. J. Cereb. Blood Flow Metab. 27, 1563–1572. https://doi.org/10.1038/sj.jcbfm.9600462.

Stumme, J., Jockwitz, C., Hoffstaedter, F., Amunts, K., Caspers, S., 2020. Functional network reorganization in older adults: graph-theoretical analyses of age, cognition

and sex. Neuroimage 214, 116756. https://doi.org/10.1016/j.neuroimage.2020.116756.
Tomasi, D., Volkow, N.D., 2012. Aging and functional brain networks. Mol. Psychiatry 17, 549–558. https://doi.org/10.1038/mp.2011.81.
Tsvetanov, K.A., Henson, R.N.A., Tyler, L.K., Davis, S.W., Shafto, M.A., Taylor, J.R., Williams, N., Cam-Can, Rowe, J.B., 2015. The effect of ageing on fMRI: correction for the confounding effects of vascular reactivity evaluated by joint fMRI and MEG in 335 adults. Hum. Brain Mapp. 36, 2248–2269. https://doi.org/10.1002/hbm.22768.
Vaidya, J.G., Paradiso, S., Boles Ponto, L.L., McCormick, L.M., Robinson, R.G., 2007. Aging, grey matter, and blood flow in the anterior cingulate cortex. Neuroimage 37, 1346–1353. https://doi.org/10.1016/j.neuroimage.2007.06.015.
van Baarsen, K.M., Kleinnijenhuis, M., Jbabdi, S., Sotiropoulos, S.N., Grotenhuis, J.A., van Cappellen van Walsum, A.M., 2016. A probabilistic atlas of the cerebellar white matter. Neuroimage 124, 724–732. https://doi.org/10.1016/j.neuroimage.2015.09.014.
Varangis, E., Habeck, C.G., Razlighi, Q.R., Stern, Y., 2019. The effect of aging on resting state connectivity of predefined networks in the brain. Front. Aging Neurosci. 11, 234. https://doi.org/10.3389/fnagi.2019.00234.
Westlye, L.T., Walhovd, K.B., Dale, A.M., Bjørnerud, A., Due-Tønnessen, P., Engvig, A., Grydeland, H., Tamnes, C.K., Østby, Y., Fjell, A.M., 2010. Life-span changes of the human brain white matter: diffusion tensor imaging (DTI) and volumetry. Cereb. Cortex 20, 2055–2068. https://doi.org/10.1093/cercor/bhp280.
Yan, C.G., Cheung, B., Kelly, C., Colcombe, S., Craddock, R.C., Di Martino, A., Li, Q., Zuo, X.N., Castellanos, F.X., Milham, M.P., 2013. A comprehensive assessment of regional variation in the impact of head micromovements on functional connectomics. Neuroimage 76, 183–201. https://doi.org/10.1016/j.neuroimage.2013.03.004.
Yan, C.G., Wang, X.D., Zuo, X.N., Zang, Y.F., 2016. DPABI: data processing & analysis for (Resting-State) Brain Imaging. Neuroinformatics 14, 339–351. https://doi.org/10.1007/s12021-016-9299-4.
Yang, C., Zhang, W., Yao, L., Liu, N., Shah, C., Zeng, J., Yang, Z., Gong, Q., Lui, S., 2020. Functional alterations of white matter in chronic never-treated and treated schizophrenia patients. J. Magn. Reson. Imaging 52, 752–763. https://doi.org/10.1002/jmri.27028.
Yeo, B.T.T., Krienen, F.M., Sepulcre, J., Sabuncu, M.R., Lashkari, D., Hollinshead, M., Roffman, J.L., Smoller, J.W., Zöllei, L., Polimeni, J.R., Fischl, B., Liu, H., Buckner, R. L., 2011. The organization of the human cerebral cortex estimated by intrinsic functional connectivity. J. Neurophysiol. 106, 1125–1165. https://doi.org/10.1152/jn.00338.2011.
Yu, M., Linn, K.A., Cook, P.A., Phillips, M.L., McInnis, M., Fava, M., Trivedi, M.H., Weissman, M.M., Shinohara, R.T., Sheline, Y.I., 2018. Statistical harmonization corrects site effects in functional connectivity measurements from multi-site fMRI data. Hum. Brain Mapp. 39, 4213–4227. https://doi.org/10.1002/hbm.24241.
Zhao, Y., Gao, Y., Li, M., Anderson, A.W., Ding, Z., Gore, J.C., 2022a. Functional parcellation of human brain using localized topo-connectivity mapping. IEEE Trans. Med. Imaging 1. https://doi.org/10.1109/TMI.2022.3168888.
Zhao, Y., Gao, Y., Zu, Z., Li, M., Schilling, K.G., Anderson, A.W., Ding, Z., Gore, J.C., 2022b. Detection of functional activity in brain white matter using fiber architecture informed synchrony mapping. Neuroimage 258, 119399. https://doi.org/10.1016/j.neuroimage.2022.119399.
Zonneveld, H.I., Pruim, R.H.R., Bos, D., Vrooman, H.A., Muetzel, R.L., Hofman, A., Rombouts, S.A.R.B., van der Lugt, A., Niessen, W.J., Ikram, M.A., Vernooij, M.W., 2019. Patterns of functional connectivity in an aging population: the Rotterdam study. Neuroimage 189, 432–444. https://doi.org/10.1016/j.neuroimage.2019.01.041.